RESEARCH ARTICLE | JUNE 24 2020

Experimental determination of electron attenuation lengths in complex materials by means of epitaxial film growth: Advantages and challenges

Special Collection: Special Topic Collection: Reproducibility Challenges and Solutions

Scott A. Chambers; Yingge Du

Journal of Vacuum Science & Technology A 38, 043409 (2020)
https://doi.org/10.1116/6.0000291
CHORUS

JVST A
Journal of Vacuum Science & Technology A

ARTICLE

avs.scitation.org/journal/jva

Experimental determination of electron attenuation lengths in complex materials by means of epitaxial film growth: Advantages and challenges

Cite as: J. Vac. Sci. Technol. A 38, 043409 (2020); doi: 10.1116/6.0000291
Submitted: 1 May 2020 · Accepted: 4 June 2020 ·
Published Online: 24 June 2020

Scott A. Chambers[a] and Yingge Du

AFFILIATIONS

Physical and Computational Sciences Directorate Pacific Northwest National Laboratory Richland Washington 99352

Note: This paper is part of the Special Topic Collection on Reproducibility Challenges and Solutions.
[a]**Electronic mail:** sa.chambers@pnnl.gov

ABSTRACT

Accurate electron attenuation lengths are of critical importance in using electron spectroscopic methods to quantitatively characterize complex materials. Here, the authors show that analysis of core-level and valence-band x-ray photoelectron spectra excited with monochromatic AlKα x-rays from the substrate and measured as a function of film thickness can be used to determine electron attenuation lengths in epitaxial $SrTiO_3$ films on Ge(001). Closely lattice-matched epitaxial heterojunctions are ideal systems for determining attenuation lengths provided the films grow in a layer-by-layer fashion, leading to atomically flat surfaces, and the buried interfaces are atomically abrupt. In principle, either the rate of attenuation of substrate peak intensities or the rate of increase of film peak intensities can be used for this purpose. However, the authors find that structural nonuniformities in the films reduce the accuracy of electron attenuation lengths determined from photoelectrons that originate *within* the films. A more reliable source of information is found in photoelectrons from the substrate which traverse the film. By using the energy dependence of calculated electron attenuation lengths from the NIST database in combination with Ge 3d core and Ge-derived valence-band intensities, the authors determine electron attenuation length as a function of kinetic energy for $SrTiO_3$.

I. INTRODUCTION

It is well known that electron spectroscopy is inherently surface sensitive because of strong interaction between electrons and solids. The complexities of electron-atom scattering make it difficult to accurately determine such fundamental quantities as characteristic scattering lengths, which in turn determine the sensitivity of various electron spectroscopies to depth within a given material. As a result, it is often difficult to use x-ray photoelectron spectroscopy (XPS) and its variant hard x-ray XPS (or HAXPES) to accurately characterize compositions and electronic structures of complex multicomponent materials. Useful formulas have been developed to predict inelastic mean free paths (IMFPs) for a variety of materials based on optical constants from which the probability of inelastic scattering is calculated as a function of momentum transfer.[1–4] These values have been compared to experimental results for metals based on elastic peak electron spectroscopy and differences ranging from 12% to 17% were noted.[5–9] Recent calculations based on a more sophisticated physical model containing higher-order corrections to the Penn algorithm[1] yielded better agreement with the experiment for Cu.[10] Inelastic scattering leading to signal attenuation is thought to be largely isotropic, resulting in an overall loss of intensity that scales with distance from the emitting atom to the surface.

However, it is also well known that Auger and photoelectron waves undergo elastic scattering from ion cores in the vicinity of the emitter and that the resulting interference effects can modulate measured intensities in complicated ways. The effect is particularly strong for single crystals and epitaxial films because the inherent

long-range order results in comparable interference effects at the detector for all atoms located in crystallographically equivalent sites. As a result, strong diffraction modulation is observed in angle-dependent measurements and has been extensively used to determine local structural environments of specific atoms by interpreting experimental data using well-established electron-atom scattering formalisms.[11–15] As useful as elastic scattering and interference is, it can complicate the measurement of IMFPs because the strongly anisotropic nature of the former modulates experimentally measured intensities used to determine the latter. In order to account for these elastic interactions in determining characteristic inelastic scattering lengths, two quite different theoretical methods have been developed. One involves Monte Carlo simulations based on photoionization and scattering cross sections and IMFPs (Refs. 16–18) and another less rigorous but much faster approach is based on solution to the Boltzmann equation within the transport approximation.[19] Interestingly, the two yield rather similar results. The latter has been utilized in the NIST Electron Effective Attenuation Length Database, which calculates effective electron attenuation lengths (EALs) for materials of interest. EALs are essentially IMFPs that have been approximately corrected for the effects of elastic scattering.[20] Powell[21] has written an excellent review of the basic concepts and methods of calculating IMFPs and EALs.

It is also of considerable interest to experimentally determine EALs for specific materials. The traditional way this has been attempted is to deposit thin films of known quantity on dissimilar substrates and use the attenuation (increase) of substrate (film) Auger and photoelectron peak intensities to determine EALs at the characteristic kinetic energies of various spectral features. However, these results have, in general, not been satisfactory because films often nucleate via island growth, resulting in a range of film thicknesses across the surface.[22] In the absence of detailed morphological information from scanning probe microscopy, it is not possible to model area-averaged electron spectroscopy data to determine EALs in an accurate way when island growth occurs. However, certain heteroepitaxial films can be grown in a layer-by-layer fashion under controlled conditions pertaining to lattice match, substrate temperature, and growth rate. In such cases, the root-mean-square surface roughness is less than 1 nm and scanning probe microscopy images reveal a terrace-step structure indicative of an atomically flat surface. In this case, simple models can, in principle, be used to extract accurate EALs, as has been shown previously for elemental epitaxial films of metals and semiconductors.[23,24] The problem is more difficult if the epitaxial film is a complex material with multiple sublattices.

In this paper, we take this method to the next level of difficulty by attempting to experimentally measure EALs for a prototypical complex oxide semiconductor, *n*-$SrTiO_3$ (STO), using epitaxial films deposited on *p*-Ge(001) by means of molecular beam epitaxy (MBE). We analyze XPS core-level and valence-band (VB) intensities for both STO and Ge spectral features as a function of the STO film thickness using the standard attenuation model that captures the effects of inelastic scattering at the level of the Beer–Lambert law. We do so in a way that mitigates some of the complicating effects of elastic scattering and interference inherent in epitaxial films. In order for this approach to yield accurate EALs, it is critical that the film/substrate interface be atomically abrupt, that the films grow in a layer-by-layer fashion, leading to surfaces with root-mean-square roughnesses that are negligibly small compared to the film thicknesses, and that the films have consistent, uniform structure and composition throughout. The first two of these three criteria are met in the STO/Ge(001) system. We show that the presence of antiphase boundaries (APBs) in the films resulting from the growth sequence required to achieve heteroepitaxy without GeO_2 formation at the interface, together with thickness-dependent photoelectron diffraction effects, complicates the analysis for peaks originating in the STO film. We also show that these effects can be at least partially mitigated by using the attenuation of Ge XPS intensities rather than the increase of STO XPS intensities.

II. EXPERIMENT

Ga-doped *p*-Ge(001) substrates ($\rho = 0.04\,\Omega\,cm$) were etched using four cycles of dipping in 15% HCl and 7% H_2O_2. The substrates were then rinsed in de-ionized water and immediately loaded to the system loadlock. The surface oxide was desorbed by heating in the MBE chamber to ~600 °C, resulting in a clean, well-ordered *p*-Ge(001)-(2×1) surface.

Oxygen-vacancy-doped STO(001) epitaxial films were deposited using molecular beam epitaxy following the approach outlined in Jahangir-Moghadam *et al.*[25] Deposition of 0.5 ML Sr at a substrate temperature of 400 °C in ultrahigh vacuum was first done to generate an oxidation-resistant $SrGe_2$(001) (3×1) template layer. Upon cooling the substrate to ~25 °C, oxygen was admitted into the growth chamber at a flow rate of 0.3 sccm and a chamber pressure of 4×10^{-7} Torr. 2.5 ML Sr and 3.0 ML Ti were then coevaporated, resulting in a 3 u.c. thick disordered STO film. The chamber was then purged of O_2 and the sample temperature was ramped to ~600 °C or until the film crystallized as evidenced by the appearance of a sharp reflection high-energy electron (RHEED) diffraction pattern, whichever came first. For films thicker than 3 u.c., additional monolayers of Ti and Sr were codeposited in progressively higher O_2 partial pressures and substrate temperatures up to 600 °C, followed by vacuum annealing for enhanced crystallization. Additional details can be found elsewhere.[26]

In situ XPS and x-ray photoelectron diffraction (XPD) measurements were performed at normal emission using a Scienta Omicron R3000 analyzer and a monochromatic AlKα x-ray source ($h\nu = 1487$ eV) with an energy resolution of ~0.4 eV. The binding energy scale was calibrated using the Ag $3d_{5/2}$ core level (368.21 eV) and the Fermi level from a polycrystalline Ag foil.

III. RESULTS AND DISCUSSION

A. Methodology

Consider a set of spectra measured at some polar angle relative to the surface normal, θ, for an epitaxial film of thickness t deposited on a clean, well-ordered substrate. The effective EAL (λ) at the kinetic energy of a given spectral feature originating in the substrate with intensity $I_{sub}(t, \theta)$ can be expressed assuming exponential decay of the intensity with increasing t in a simple continuum

model as

$$\lambda = \frac{\left(-\frac{t}{\cos\theta}\right)}{\ln\left[\frac{I_{sub}(t,\theta)}{I_0}\right]}. \quad (1)$$

Likewise, the analogous formula for a film peak with intensity $I_{film}(t, \theta)$ is

$$\lambda = \frac{\left(-\frac{t}{\cos\theta}\right)}{\ln\left[1 - \frac{I_{film}(t,\theta)}{I_\infty}\right]}. \quad (2)$$

Here, I_0 and I_∞ are the intensities from a clean substrate (i.e., $t = 0$) and a film of thickness much greater than λ, respectively. In this approach, the essential criterion for the thick film is that the substrate peaks are not detectable, a condition automatically fulfilled for $>\sim 4.6\lambda$ (99% attenuation). It is important to note that λ values extracted from Eq. (1) are influenced by inelastic scattering in both the substrate and the film whereas those from Eq. (2) are determined solely by attenuation in the film. Equation (1) thus yields a weighted average of the EALs of the substrate and film material, the weighting coefficients being dependent on the film thickness. As mentioned above, XPD and Auger photoelectron diffraction effects can modulate measured intensities by a few to several tens of percent, depending on the crystalline quality of the sample and the angular acceptance of the energy analyzer. We illustrate this result in Fig. 1, where we show core-level XPS intensities as a function of azimuthal (a) and polar (b) angles for bulk STO(001). The primary dataset was measured using an analyzer acceptance cone of full angle equal to 14°. Here, we see that the Sr 3d (kinetic energy, $E_k = 1348$ eV), Ti $2p_{3/2}$ ($E_k = 1023$ eV), and O 1s ($E_k = 952$ eV) intensity profiles exhibit substantial interference-induced modulation across angle space. Notably, strong so-called "forward focusing" intensity enhancements[27] are seen along the close-packed [011] and [001] directions for all three core levels in panel b. These features, which are universal for E_k values in excess of ~100 eV, are essentially 0th-order diffraction peaks originating from strong Coulomb interaction of the photoelectron wave with the ion cores along the exit trajectory for which the scattering phase shifts are small.[12] The [101] and symmetry-equivalent family of features fall every 90° in the O1s azimuthal scan at a polar angle of 45° shown in panel a, as expected for a cubic perovskite lattice. The intensity enhancement along [001], defined as $\Delta I/I_{[001]}$ where ΔI is the intensity change from $\theta = 0°$ to $\theta = \pm 10°$ in any azimuthal direction, is 27%, 29%, and 29% for Sr 3d, Ti $2p_{3/2}$, and O 1s, respectively. Significantly, the fact that this variation is nearly the same for all three core levels indicates that XPD effects are comparable in spectra measured along the surface normal for film thicknesses of several unit cells (u.c.) or more. We thus base our analysis on spectra measured along [001], a convenient choice because it is also quite straightforward to reproducibly orient the sample along the surface normal. Finally, we note that increasing the acceptance cone to 30° reduces but does not eliminate XPD effects, as seen in the second O 1s polar scan measured with this instrument setting in panel b. Therefore, diffraction effects must be taken into consideration due to the finite angular resolution of all commercially available hemispherical analyzers.

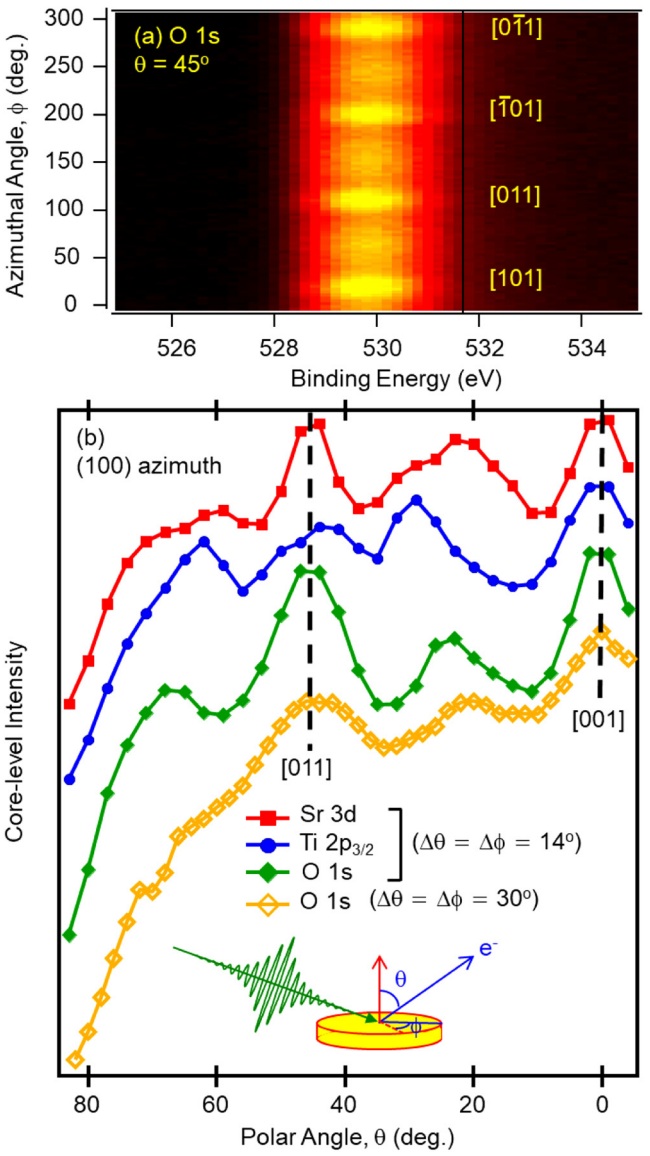

FIG. 1. X-ray photoelectron diffraction data for bulk *n*-$SrTiO_3$(001) including an azimuthal scan of the O 1s intensity at a polar angle of 45° (a), and polar scans of the Sr 3d, Ti $2p_{3/2}$, and O 1s intensities in the (100) azimuth (b). The individual polar scans have been offset along the ordinate for clear viewing. The effect of angular acceptance is illustrated for the O 1s core level in the polar scan.

B. Core-level and valence-band spectral analysis

Figure 2 shows core-level spectra measured at normal emission for a set of epitaxial STO films on Ge(001). The line shapes

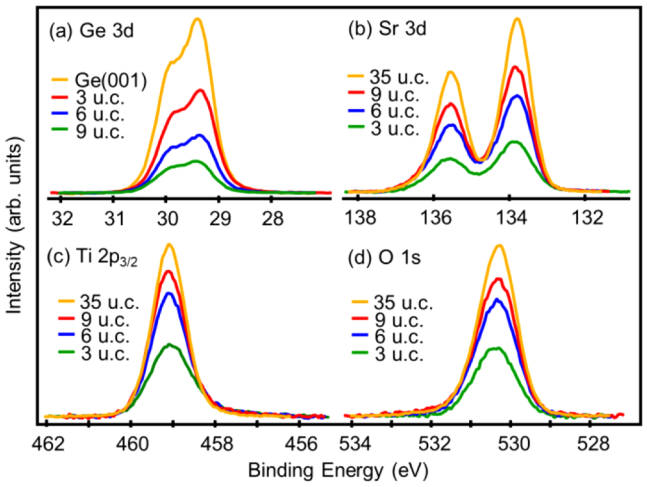

FIG. 2. Ge 3d (a), Sr 3d (b), Ti $2p_{3/2}$ (c), and O 1s (d) core-level spectra measured at normal emission for $SrTiO_3$/Ge(001) heterojunctions. One u.c. is equivalent to ~3.7–3.9 Å along the growth direction for epitaxial $SrTiO_3$ on Ge(001), depending on the extent of relaxation.

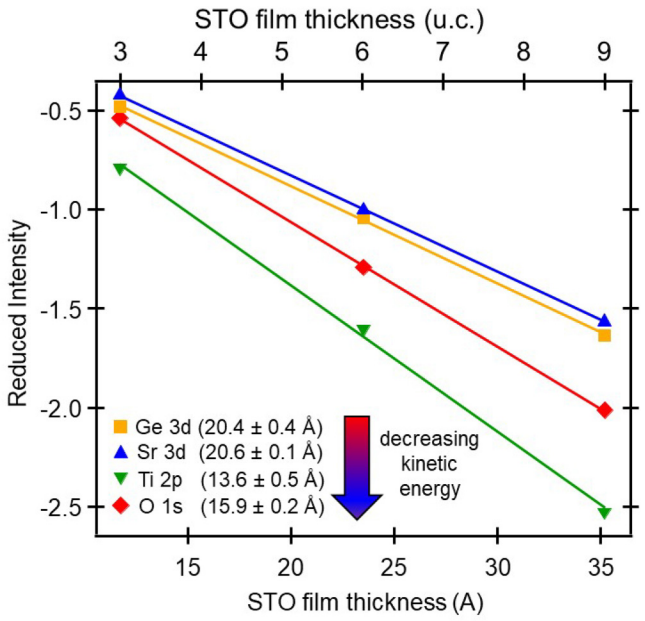

FIG. 3. Reduced intensities for Ge 3d, Sr 3d, Ti $2p_{3/2}$, and O 1s core-level spectra measured at normal emission (see Fig. 2) vs film thickness. The numbers in parentheses are the measured EALs and are numerically equal to the negative inverse slopes according to Eqs. (1) and (2).

for the heterojunctions (HJs) are largely unchanged relative to those measured for the phase-pure reference materials, the exception being Ge 3d ($E_k = 1453$ eV). Ge 3d spectra show a subtle broadening not seen in the spectrum for clean p-Ge(001)-(2×1) due the presence of built-in potentials in the underlying Ge; the Sr 3d, Ti2$p_{3/2}$, and O 1s line shapes are the same as those for bulk STO.[26] These results reveal that secondary phase formation due to interface reactivity does not occur. Additionally, STEM images show that the interface is atomically abrupt. However, STEM also shows that two distinct interface structures occur on opposite sides of APBs in the films[26] and this fact complicates the analysis for thinner films, as shown below. The film (substrate) peak intensities increase (decay) with film thickness in the manners expected for layer-by-layer film growth and no atomic mixing at the interface, and STEM, reflection high-energy electron diffraction and scanning probe microscopy reveal that the film surfaces are atomically flat.

The reduced intensities, defined as $\ln\left[\frac{I_{sub}(t,\theta)}{I_0}\right]$ and $\ln\left[1-\frac{I_{film}(t,\theta)}{I_\infty}\right]$ for the substrate and film peaks, respectively, are plotted against film thickness in Fig. 3. The negative reciprocals of the slopes as determined by linear regression should yield the effective EALs at the E_k values of the different core levels. In order of decreasing E_k, the resulting values are 20.4(4), 20.6(1), 13.6(5), and 15.9(2) Å for Ge 3d, Sr 3d, Ti2$p_{3/2}$, and O 1s, respectively, with the numbers in parentheses being the uncertainties in the last digit. The associated r^2 correlation coefficients are 0.99964, 0.99998, 0.99842, and 0.99995, respectively. Despite the near-unity correlation values, these EAL values do not vary monotonically with E_k, as would be expected based on theoretical predictions discussed below.

We also determine λ at the maximum kinetic energy achievable using AlK α x-rays (~1480 eV) by analyzing the VB spectra for the 3, 6, and 9 u.c. HJs (Fig. 4). We model the spectra as linear combinations of VB spectra for the bulk component materials using

$$I_{HJ}(E_b) = C_1 I_{Ge}(E_b) + C_2 I_{STO}(E_b). \quad (3)$$

The component spectra are weighted by factors that depend on λ. The weighting factors (C_1 and C_2) and flat-band VB offset are treated as free parameters in the analysis. However, based on the same physical model used to derive Eqs. (1) and (2), the weighting coefficients for the Ge and STO spectra should ideally be given by $C_1 = \exp(-t/\lambda)$ and $C_2 = 1 - \exp(-t/\lambda)$, respectively, provided two conditions are met. First, these formulas assume that the heterojunction spectrum is composed entirely of contributions from the phase-pure components and that no interface phase is present. Second, all spectra must be measured with the same instrument parameters, including incident x-ray brightness, pass energy, slit width, detector voltage, and sample position. If either of these two conditions is not met, Eq. (3) with the definitions of C_1 and C_2 given above will not hold, and a reliable λ value will not result. If these conditions are perfectly met, then an excellent fit yielding a single value of λ should occur, and the boundary condition $C_1 + C_2 = 1$ should be met. The optimal simulations are shown in Fig. 4 and the resulting numerical values are given in Table I. As seen in the figure, very good fits are achieved for all film thicknesses. As seen in Table I, the λ values taken individually from C_1 and C_2 are highly reproducible from sample to sample but differ from one another by a significant amount. Moreover $C_1 + C_2$ is less than unity. These nonidealities are not due to instrumental issues. The

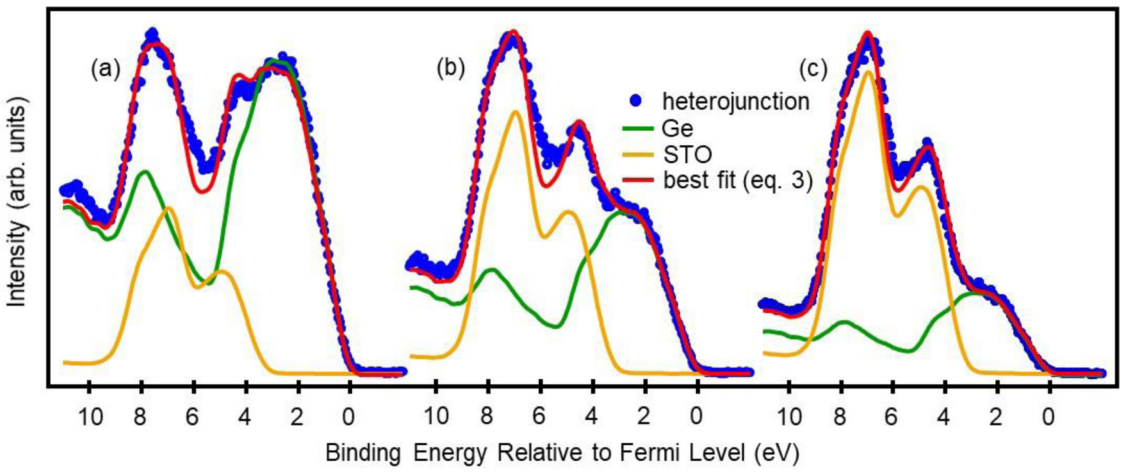

FIG. 4. VB spectra measured at normal emission for n u.c. $SrTiO_3$/Ge(001) heterojunctions with n equal to 3 (a), 6 (b), and 9 (c). Also shown are simulations consisting of linear combinations of VB spectra for pure p-Ge(001)-(2 × 1) and n-$SrTiO_3$(001) with optimized energy offsets and weighting factors. The weighting factors for Ge and $SrTiO_3$ can be expressed as $C_1 = \exp(-t/\lambda)$ and $C_2 = 1 - \exp(-t/\lambda)$, respectively, and used to extract a λ value for the VB kinetic energy under conditions given in the text.

three spectra were measured over a period of a few days and decay of the x-ray intensity due to anode wear is negligible over this period of time. Additionally, sample positioning is highly reproducible in our spectrometer and no change was made to the spectrometer settings. Therefore, instrumental factors are not likely the cause for the difference from C_1 and C_2 for a given sample. Rather, we hypothesize that the EAL values from C_2 are not reliable because of structural variations within the STO films, as discussed below. We thus determine λ at the VB kinetic energy using C_1. Doing so yields arithmetic mean and standard deviation of 21.0 ± 0.05 Å at $E_k = 1480$ eV.

C. Merging with theoretical predictions

We plot all measured EALs as a function of kinetic energy in Fig. 5 along with calculated values from the NIST Electron Effective Attenuation Length Database (V1.3).[20] In contrast to the experimental data, the calculated EALs are very well fit to a straight line over the kinetic energy range of interest (900–1500 eV). The two closely spaced Ge-derived EAL values (VB C_1 and Ge 3d) exhibit the same energy dependence (i.e., slope) as the calculated values but are ~2 Å lower. We hypothesize that the nonmonotonic behavior in the λ values derived from the Sr 3d, Ti 2p and O 1s spectra is caused by structural heterogeneities in the films, specifically related to the presence of APBs.[26] APBs result in stacking faults that produce a mixed surface termination.[28] Stacking faults have also been shown to be accompanied by inequivalent interface structures resulting in nonuniformities in the local structural environments of Sr, Ti, and O near the interface.[26] As a result, the

TABLE I. Weighting coefficients and resulting electron attenuation lengths from simulating valence-band spectra for STO/Ge(001) heterojunctions.

t (u.c.)	C_1	λ (Å)	C_2	λ (Å)	$C_1 + C_2$
3	0.58	21.5	0.38	24.5	0.96
6	0.33	21.1	0.62	24.2	0.95
9	0.18	20.5	0.78	23.2	0.96

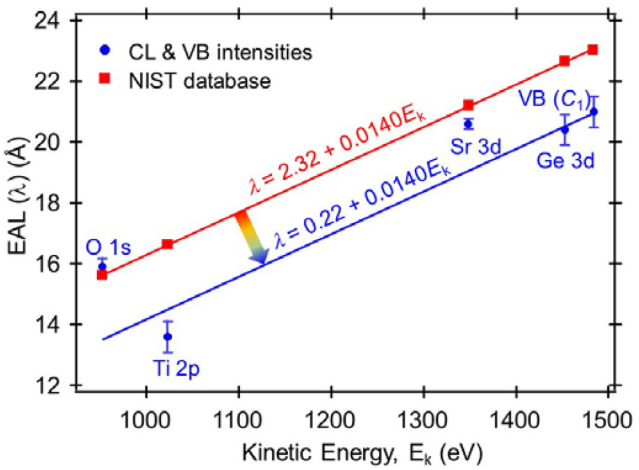

FIG. 5. Measured (circles) and calculated (circles) electron attenuation lengths for $SrTiO_3$. The experimental values were determined using Eqs. (1) and (2) (core levels) and the VB analysis [Eq. (3)] summarized in Fig. 3. The linear fit to the calculated values (upper line) was transposed with the same slope to intersect with experimental Ge 3d and VB EAL values (lower line) in order to obtain extrapolated λ values at the kinetic energies of the Sr 3d, Ti $2p_{3/2}$, and O 1s core levels.

photoelectron intensities from inequivalent Ti, Sr, and O sites in these different interfacial structures will not be the same, particularly for the 3 u.c. film for which the interfacial region is the largest fraction of the total film volume. This effect alters Ti 2p, Sr 3d, and O1s intensities relative to what is expected from a single, thickness independent STO film structure. Additionally, Eq. (2) is expected to yield accurate values of λ only if all films have the same surface termination (either SrO, TiO_2, or an invariant mix of the two). Indeed, the Ti 2p-to-Sr 3d peak area ratio measured at normal emission decreases by ~20% in changing the surface termination of STO(001) from the TiO_2 plane to the SrO plane.[28] As a result, significant error is introduced into the EALs based on Eq. (2) if the mix of the different surface terminations is not the same in all films. These structural complexities are a byproduct of the method that was used to grow epitaxial STO on Ge(001). Specifically, the first few u.c. were deposited as a disordered film onto a single monolayer of $SrGe_2$ with the substrate near room temperature in order to avoid forming GeO_2 at the interface,[25] similar to the method used to grow STO on Si(001) without SiO_2 formation.[29] The amorphous thin film was then crystallized by heating in ultrahigh vacuum followed by growing additional epitaxial STO at a higher substrate temperature. APBs presumably form in the film during the crystallization process.

The nature of the problem described above can be illustrated by comparing our experimental data to model calculations as shown in Fig. 6. Here, we compare the measured Ti $2p_{3/2}$-to-Sr 3d peak area ratio as a function of film thickness to calculated sums of intensities over discrete layers for the two surface terminations. For a TiO_2-terminated film consisting of n unit cells, this intensity ratio

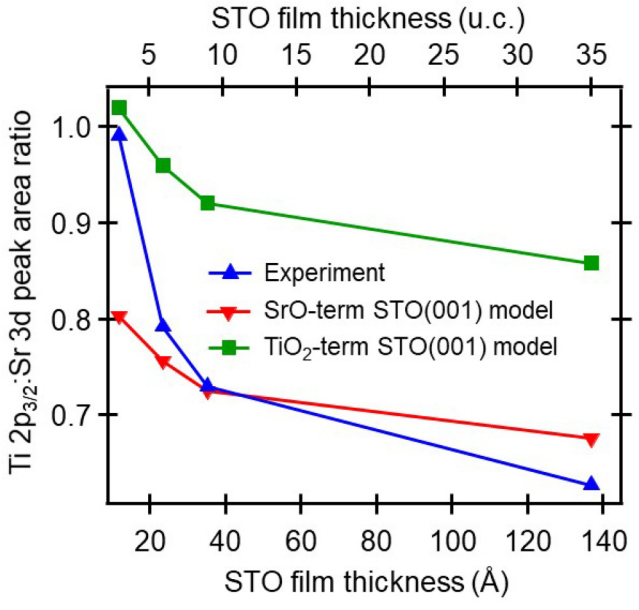

FIG. 6. Measured and calculated [Eqs. (4) and (5)] Ti $2p_{3/2}$-to-Sr 3d core-level intensity ratios vs film thickness for $SrTiO_3$/Ge(001) heterojunctions.

can be expressed as

$$\left[\frac{I_{\mathrm{Ti\ 2p}}(t,\theta)}{I_{\mathrm{Sr\ 3d}}(t,\theta)}\right]_{\mathrm{TiO_2}} \propto \frac{\sum_{i=1}^{n}\exp\left(\frac{-ic}{\lambda_{\mathrm{Ti\ 2p}}\cos\theta}\right)}{\sum_{i=1}^{n}\exp\left(\frac{-(i+0.5)c}{\lambda_{\mathrm{Sr\ 3d}}\cos\theta}\right)}. \quad (4)$$

Here, c is the out-of-plane lattice parameter (3.905 Å for STO) and all other parameters are defined above. Analogously, the same intensity ratio for an SrO-terminated film of thickness n u.c. is

$$\left[\frac{I_{\mathrm{Ti\ 2p}}(t,\theta)}{I_{\mathrm{Sr\ 3d}}(t,\theta)}\right]_{\mathrm{SrO}} \propto \frac{\sum_{i=1}^{n}\exp\left(\frac{-(i+0.5)c}{\lambda_{\mathrm{Ti\ 2p}}\cos\theta}\right)}{\sum_{i=1}^{n}\exp\left(\frac{-ic}{\lambda_{\mathrm{Sr\ 3d}}\cos\theta}\right)}. \quad (5)$$

The spectrometer transmission function has nearly the same value at the Ti 2p and Sr 3d kinetic energies for our analyzer and thus does not affect these ratios. The EAL values used in the model calculations from Eqs. (4) and (5) are taken from the linear extrapolation of our Ge 3d and VB data summarized in Fig. 5 (see discussion below) and are 19.1 Å for Sr 3d and 14.5 Å for Ti 2p. However, the conclusions we reach are independent of the specific λ values. Looking first at the model predictions in Fig. 6, the peak area ratio decreases with increasing t, as expected because the contribution of the surface layer to the total intensity becomes less important as the total number of layers goes up. While the experimental results qualitatively follow this trend, the magnitude of the change with t is much larger, particularly in going from 3 to 6 u.c. All four films were grown in the same way by MBE with careful calibration between extended flux monitoring and RHEED oscillations from STO homoepitaxy, resulting in phase-pure STO films in which the Sr-to-Ti atom ratio differs from 1:1 by at most a few percent. We thus conclude that the nonmonotonic scatter in the EALs taken from the film peaks is most likely due to some combination of variable stacking fault density from film to film, leading to different proportions of TiO_2- and SrO-terminated domains, and varying photoelectron diffraction effects from structurally inequivalent sites near the interface.

In contrast to STO, clean Ge(001)-(2 × 1) has a single sublattice and a well-defined surface structure on which the STO is grown. Ge photoelectrons penetrate and traverse the STO film *as a block* and are inelastically scattered in ways that are controlled by the properties of that block, namely, film thickness, bandgap, and carrier concentration. The validity of this statement requires that each member of the STO film set has nearly the same volume-averaged composition from film to film, and this condition is fulfilled here because of careful flux monitoring. As a result, we have greater confidence in the EALs from Ge 3d intensities generated by Eq. (1) along with the C_1 values for the VB spectrum analysis than we do in those determined from Eq. (2) based on the STO core-level intensities and C_2 values from the VB spectrum analysis. Because the Ge 3d attenuation rate yields a weighted average of the EAL values for Ge and STO, it is important to determine if additional error is incurred in the EAL for STO by including the contribution from Ge. Since we cannot isolate the contributions from Ge

and STO in the experimental results, we again turn to the NIST database.[20] Analysis based on these numbers yields 22.5 Å for Ge 3d photoelectrons traversing the Ge below all STO films and 23.2 to 22.7 Å for the same photoelectrons passing through STO films of thickness 3 to 9 u.c. These values are sufficiently similar that we conclude that negligible additional error is incurred by this unavoidable averaging.

In order to generate more reasonable λ values at the kinetic energies of the Sr 3d, Ti 2p, and O1s core levels, we take the energy dependence (i.e., slope) from the linear regression of the NIST database results and use it to extrapolate from the Ge 3d and VB kinetic energies down to 950 eV. Reducing the y-intercept of the upper regression line equation for the fit to the NIST values by 2.0 Å results in the lower line that straddles the Ge 3d and VB data points seen in Fig. 5. This line yields EAL values of 19.1, 14.5, and 13.5 Å for at the Sr 3d, Ti 2p, and O 1s kinetic energies, respectively. The 2 Å difference between these experimental EAL values for epitaxial STO/Ge(001) and those calculated in the NIST database is due to the fact that the latter are computed in the absence of a single-crystal orientation. Elastic scattering is taken into account in the NIST calculations in an approximate way by computing a parameter known as the single-scattering albedo. This atom-specific parameter is calculated for each element in the material and then averaging over all elements therein. In contrast, the experiment was carried out for epitaxial films of a single orientation at a particular emission angle relative to the crystal axes. Therefore, the elastic scattering that each kind of photoelectron undergoes is not accurately represented by an average over elements and angles. Indeed, accurately accounting for the diffraction modulation in the experiment requires a multiple scattering formalism in which the atomic coordinates are accurately known (by fitting theory and experiment) and thermal diffuse scattering is properly incorporated via Debye–Waller factors.[11–15]

IV. SUMMARY AND CONCLUSIONS

Analysis of core-level and valence-band XPS intensities for a series of epitaxial $SrTiO_3$ films on Ge(001) was carried out with the goal of extracting the kinetic energy dependence of the effective electron attenuation length in $SrTiO_3$. Experimental data have been interpreted using simple continuum equations based on the assumption of isotropic, exponential intensity attenuation via inelastic scattering. EALs from core levels originating in the epitaxial films do not exhibit the expected monotonic dependence on kinetic energy, suggesting that photoelectron diffraction in concert with nonuniformities in the films affect measured intensities in ways that preclude the use of simple models. Rather, EALs from substrate spectral features, combined with a theoretical energy dependence, were extrapolated to lower kinetic energies to obtain EALs for the film core-level peaks. This investigation highlights the fact that although heteroepitaxial interfaces are an ideal way to determine attenuation lengths, the subtleties of the nucleation and growth of complex materials on substrates of lower symmetry can result in structural nonuniformities that can preclude using XPS data from the film, at least as interpreted with simple models.

ACKNOWLEDGMENTS

The authors are grateful to Don Baer (PNNL) for a critical reading of this manuscript. This work was supported by the U.S. Department of Energy (DOE), Office of Science, Division of Materials Sciences and Engineering under Award No. 10122 and was performed in the Environmental Molecular Sciences Laboratory, a national scientific user facility sponsored by the Department of Energy's Office of Biological and Environmental Research and located at PNNL.

REFERENCES

[1]D. R. Penn, Phys. Rev. B **35**, 482 (1987).
[2]H. Shinotsuka, S. Tanuma, C. J. Powell, and D. R. Penn, Surf. Interface Anal. **47**, 871 (2015).
[3]H. Shinotsuka, S. Tanuma, C. J. Powell, and D. R. Penn, Surf. Interface Anal. **51**, 427 (2019).
[4]H. Shinotsuka, S. Tanuma, C. J. Powell, and D. R. Penn, Surf. Interface Anal. **47**, 1132 (2015).
[5]C. J. Powell and A. Jablonski, J. Phys. Chem. Ref. Data **28**, 19 (1999).
[6]W. S. M. Werner, C. Tomastik, T. Cabela, G. Richter, and H. Stori, Surf. Sci. **470**, L123 (2000).
[7]W. S. M. Werner, C. Tomastik, T. Cabela, G. Richter, and H. Stori, J. Electron. Spectrosc. Relat. Phenom. **113**, 127 (2001).
[8]S. Tanuma, T. Shiratori, T. Kimura, K. Goto, S. Ichimura, and C. J. Powell, Surf. Interface Anal. **37**, 833 (2005).
[9]S. Tanuma, C. J. Powell, and D. R. Penn, Surf. Interface Anal. **43**, 689 (2011).
[10]P. de Vera and R. Garcia-Molina, J. Phys. Chem. C **123**, 2075 (2019).
[11]C. S. Fadley, Prog. Surf. Sci. **16**, 275 (1984).
[12]S. A. Chambers, Adv. Phys. **40**, 357 (1991).
[13]C. S. Fadley, in *Synchrotron Radiation Research: Advances in Surface and Interface Science*, edited by R. Z. Bachrach (Plenum, New York, 1992), Vol. 1, p. 421.
[14]D. P. Woodruff, J. Electron. Spectrosc. Relat. Phenom. **178**, 186 (2010).
[15]D. P. Woodruff, in *Encyclopedia of Interfacial Chemistry*, edited by K. Wandelt (Elsevier, 2018), Vol. 1.1, p. 372.
[16]C. J. Powell and A. Jablonski, Surf. Interface Anal. **33**, 211 (2002).
[17]A. Jablonski and C. J. Powell, Surf. Sci. Rep. **47**, 35 (2002).
[18]A. Jablonski, Surf. Sci. **688**, 14 (2019).
[19]A. Jablonski and C. J. Powell, J. Electron. Spectrosc. Relat. Phenom. **199**, 27 (2015).
[20]C. J. Powell and A. Jablonski, NIST Electron Effective-Attenuation-Length Database, Version 1.3, Standard Reference Data Program Database 82, U.S. Department of Commerce (National Institute of Standards and Technology, Gaithersburg, MD, 2011), see https://www.nist.gov/srd/nist-standard-referencedatabase-82.
[21]C. J. Powell, J. Vac. Sci. Technol. A **38**, 023209 (2020).
[22]J. A. Venables, G. D. T. Spiller, and M. Hanbucken, Rep. Prog. Phys. **47**, 399 (1984).
[23]S. A. Chambers, T. R. Greenlee, C. P. Smith, and J. H. Weaver, Phys. Rev. B **32**, 4245 (1985).
[24]S. A. Chambers, J. Vac. Sci. Technol. A **7**, 2459 (1989).
[25]M. Jahangir-Moghadam, K. Ahmadi-Majlan, X. Shen, T. Droubay, M. Bowden, M. Chrysler, D. Su, S. A. Chambers, and J. H. Ngai, Adv. Mater. Interfaces **2**, 1400497 (2015).
[26]Y. Du, P. V. Sushko, S. R. Spurgeon, M. E. Bowden, J. M. Ablett, T.-L. Lee, N. F. Quackenbush, J. C. Woicik, and S. A. Chambers, Phys. Rev. Mater. **2**, 094602 (2018).
[27]W. F. Egelhoff, Crit. Rev. Solid State Mater. Sci. **16**, 213 (1990).
[28]S. A. Chambers and P. V. Sushko, Phys. Rev. Mater. **3**, 125803 (2019).
[29]R. A. McKee, F. J. Walker, and M. F. Chisholm, Phys. Rev. Lett. **81**, 3014 (1998).